The role of CO_2 in CH_4 exsolution from deep brine: Implications for geologic carbon sequestration

Curtis M. Oldenburg[1]

Christine Doughty

Nicolas Spycher

Earth Sciences Division

Lawrence Berkeley National Laboratory

[1]contact: cmoldenburg@lbl.gov

May 31, 2013

Revised August 2, 2013

Abstract

The partial pressure exerted by dissolved CO_2 in water (aqueous phase) containing dissolved CH_4 at concentrations near-saturation can lead to the formation of a CH_4-rich gas phase. We have used numerical simulation with TOUGH2/EOS7C to investigate the process of CH_4 exsolution caused by CO_2 injection for geologic carbon sequestration. We validated the solubility model in TOUGH2/EOS7C against published measurements of solubility and corresponding Henry's Law coefficients. We verified our simulation results against a previously published 1D test problem, and investigated the effects of numerical dispersion on the CH_4 exsolution and flow processes. In 2D radial simulations of a model system, we found that highly concentrated CH_4 gas regions form at the leading edge of the CO_2 injection front. Because the gas saturations are small in the CH_4-rich gas regions in the generic system studied here, (1) CH_4 exsolution does not appear to be a problem for seismic monitoring of CO_2 plumes, (2) reservoir pressurization due to dilution of supercritical CO_2 by CH_4 does not appear to be a concern, and (3) relative permeability to water is not strongly reduced.

Introduction

From the perspective of demonstrated reservoir integrity, some of the most promising targets for geologic carbon sequestration (GCS) are depleted oil and gas reservoirs that have accumulated buoyant hydrocarbons over millions of years. In these systems, methane (CH_4) is ubiquitous as a major component in the gas phase, as a dissolved component in both the oil phase (if any) and the aqueous phase. Even in formations without economic hydrocarbon accumulations nearby, CH_4 is often present as a dissolved species in deep aquifers, some of which have been of interest as targets of natural gas extraction (1). These deep saline aquifers are also of great interest for GCS (2). One question that arises is what happens when CO_2 is injected into deep saline formations that contain dissolved CH_4 at or near (chemical) saturation (i.e., at or near the CH_4 concentration above which a CH_4-rich gas would exsolve).

The first-order effect of the addition of CO_2 to water containing dissolved CH_4 at or very near saturation is the evolution of a CH_4-rich gas phase (3). This process, explained here in Section 3, is expected to occur in CH_4-saturated aquifers when CO_2 is injected for GCS. Some potential impacts of the exsolution of CH_4 are (i) decreased precision of seismic monitoring of the size of the CO_2 plume due to inability to distinguish between the injected CO_2 and exsolved CH_4 gas, (ii) increased pressurization (i.e., increase in compressibility factor, Z, where $PV = ZnRT$) of the stored supercritical CO_2 as it mixes with CH_4 (4, 5), and (iii) decreased relative permeability for water due to the evolution of CH_4 gas. Regarding point (i), the contrast in seismic properties in the reservoir between brine and CO_2 or between brine and CH_4 is much larger than the contrast between CO_2 and CH_4 (e.g., Figure 2 in (6)) making it impossible at present to distinguish between CO_2 and CH_4 by surface seismic methods.

In this paper, we first present background information on prior studies that considered CH_4 in deep saline formations, and solubility studies of CO_2 and CH_4 in water. Next, we validate TOUGH2/EOS7C (7) against measured solubility data and verify the model by comparing results of CH_4 exsolution observed in another modeling study in a simple 1D test problem (3). Finally, we present results of simulations of CO_2 injection into CH_4-saturated water in a 2D radial model system to show the magnitude and locations of CH_4 exsolution and its evolution over time.

Background and Prior Work

There has been long interest in the potential for production of CH_4 from deep overpressured saline aquifers (8, 1, 9). While these reservoirs are potential energy sources by virtue of their high temperature and high CH_4 content, they are poor candidates for direct CO_2 injection for GCS because they are overpressured (aka geopressured). To address the challenges of sequestering CO_2 in geopressured systems, researchers have come up with novel concepts for coupled fluid production, energy extraction, and GCS (10). Dissolved CH_4 also occurs in many deep normally pressured reservoirs (8) that are candidates for GCS, and it is these saline formations that are the subject of this paper. In addition, the current study is relevant to deep reservoirs near or along the natural gas migration pathway to shallower natural gas reservoirs, and to aquifers near depleted natural gas reservoirs that will naturally contain large amounts of dissolved CH_4.

We previously investigated the effects of residual gas including CH_4 gas on CO_2 injection for GCS (11). The present study extends our work to consider the case of injection of CO_2 into single-phase water containing dissolved CH_4. In this case, CO_2 dissolution, and the associated increase in partial pressure exerted by the dissolved gases in particular, leads to the exsolution of CH_4 into the gas phase. While this phenomenon has been pointed out and simulated in a 1D domain (3), this prior study did not attempt to quantify or address the underlying implications of the effect for GCS. A more recent study examined both dissolved and residual-gas CH_4 effects on CO_2 injection by means of an analytical solution with emphasis on comparison of the analytical solution to numerical simulation results in terms of two-phase flow effects and relative permeability including hysteresis (12).

With the critical importance of dissolution and exsolution in controlling the flow and transport processes of interest in the general area of hydrocarbon production, a large amount of research has been carried out focused on gas solubility in water (4, 13, 14, 15, 16, 17). Most relevant to the topic of CH_4 exsolution caused by CO_2 injection is the study of Qin et al. (17) in which laboratory measurements were made of coupled solubility effects in the system H_2O-CO_2-CH_4. The Qin et al. (17) study directly addressed the effects on solubility in water of one component due to the concentration in water of the other component. As we will discuss in more detail below, Qin et al. (17) showed that the effective Henry's Law coefficient of CH_4 decreases with

dissolution of CO_2 (thus the solubility of CH_4, at a constant CH_4 partial pressure, actually increases with dissolution of CO_2). However, while the addition of CO_2 decreases the partial pressure of CH_4, it does not counter the tendency for the formation of a CH_4-rich gas phase that arises from the lower solubility of CH_4 relative to CO_2 and the sum of the partial pressures exerted by CH_4 and CO_2.

Process Modeling

In order to simulate the multiple processes involved in the injection of supercritical CO_2 into a porous medium containing water saturated with CH_4, we used TOUGH2/EOS7C (7) to model multiphase and multicomponent flow, along with multicomponent solubility including exsolution of a gas phase. TOUGH2/EOS7C uses an equilibrium constant approach to estimating Henry's Law Coefficients for each volatile component and has been tested and demonstrated on a variety of problems. However, for the subtle questions of the effects of dissolution of one component, specifically CO_2, on the solubility of a second component (CH_4), we carried out additional testing to ensure the code was capable of simulating the processes of interest in GCS in CH_4-saturated systems.

Validation of Solubility Model

The most relevant papers for our purposes of validating the equilibrium constant-based solubility model implemented in our numerical code (TOUGH2/EOS7C) were determined to be Qin et al. (17), who carried out laboratory experiments of phase equilibria in the H_2O-CO_2-CH_4 ternary system, and Kiepe et al. (15) who determined the solubility of CH_4 in pure water and electrolyte solutions. We also compared EOS7C results against CO_2 solubility in pure water and brines calculated by the methods of (18) and references therein which was shown to reproduce a large number of solubility measurements mostly within experimental error.

<u>CO_2 and CH_4 aqueous solubility (as pure components)</u>

Qin et al. (17) reported on experimental measurements of CH_4 and CO_2 mutual solubility in the two-component systems H_2O-CO_2 and H_2O-CH_4. The CO_2 solubility values reported agree closely (2–8 %) with the solubility model of (18), which was based on previously published

experimental data. We present in Figures 1a–1c comparisons of EOS7C results (version 2, using the Peng-Robinson equation of state option) with CO_2 solubility values computed with the model of (18), and in Figure 1d comparisons with the experimental CH_4 solubility values of (17) and (15) (for pure H_2O, as a function of pressure). In general, the CO_2 solubility in water calculated by EOS7C agrees well with previously published solubility data, but EOS7C appears to slightly underestimate CH_4 solubility (Figure 1d).

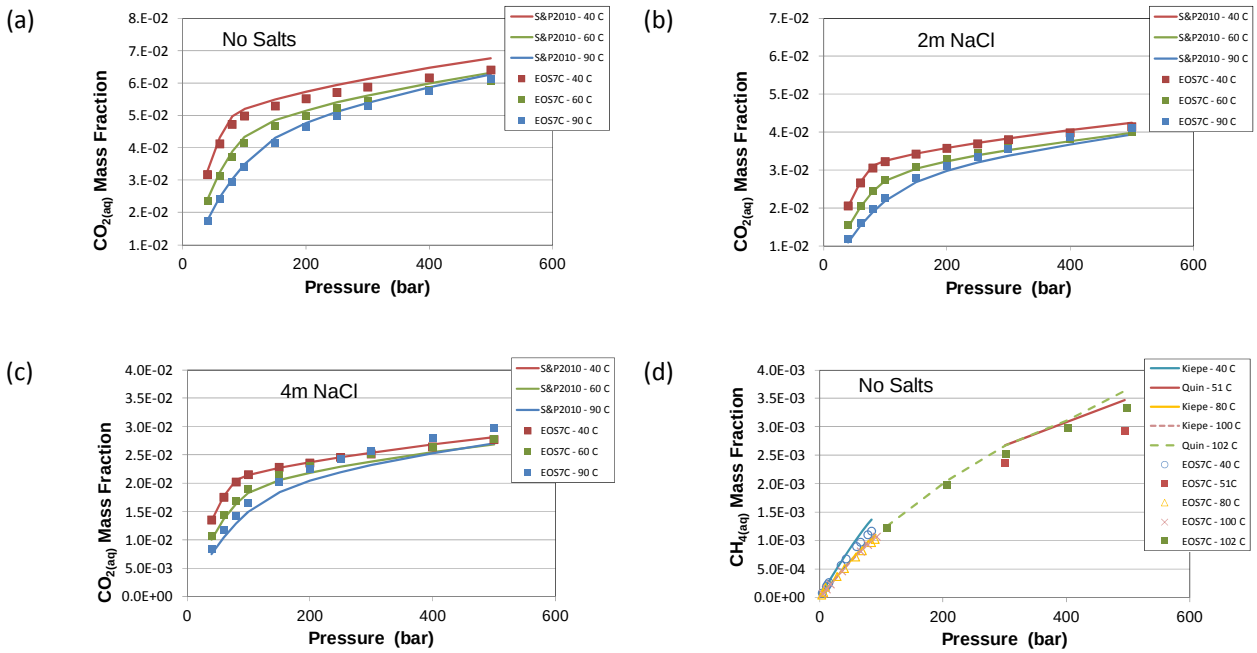

Figure 1a. Comparisons of solubility of CO_2 as a function of pressure and temperature from the literature (18), and references therein) and EOS7C for (a) pure water, (b) 2m NaCl aqueous solution, and (c) 4m NaCl aqueous solution. (d) Comparison of CH_4 solubility in pure water as a function of pressure at various temperatures computed by EOS7C and from experimental data (17, 15).

<u>Solubility in the three-component (H_2O-CO_2-CH_4) system</u>

In a multicomponent system such as H_2O-CO_2-CH_4, it is essential to model correctly the effects of each component on the solubility of the other. Example results from (17) and EOS7C are shown in Figure 2. As shown in Figure 2, the decreasing partial pressure of Component 3 (CH_4) in the gas phase with increasing molar composition of Component 2 (CO_2) indicates increased

solubility of CH_4 in the solution as the dissolved CO_2 concentration increases (for the same pressure). Such increased solubility is quantified by the effective Henry's Law coefficient given by

$$H_{CH4} = P\, y_{CH4}/x_{CH4} \qquad (1)$$

where y and x denote mole fractions in the gas and aqueous phases, respectively, and P stands for total pressure (with $P\, y_{CH4} = P_{CH4}$, the partial pressure of CH_4). Therefore, the y-axis in Figure 2 represents an effective Henry's Law coefficient. A smaller value of the Henry's Law coefficient for a component implies lower partial pressure is exerted by that component (for the same aqueous concentrations), which is equivalent to a larger solubility in the aqueous phase for that component for the same partial pressure. Note that we assume the mole fraction in the gas is approximately equal to the total mole fraction in the cell plotted in (7) on the x-axis, a good approximation given the relatively low solubilities of these gases in water.

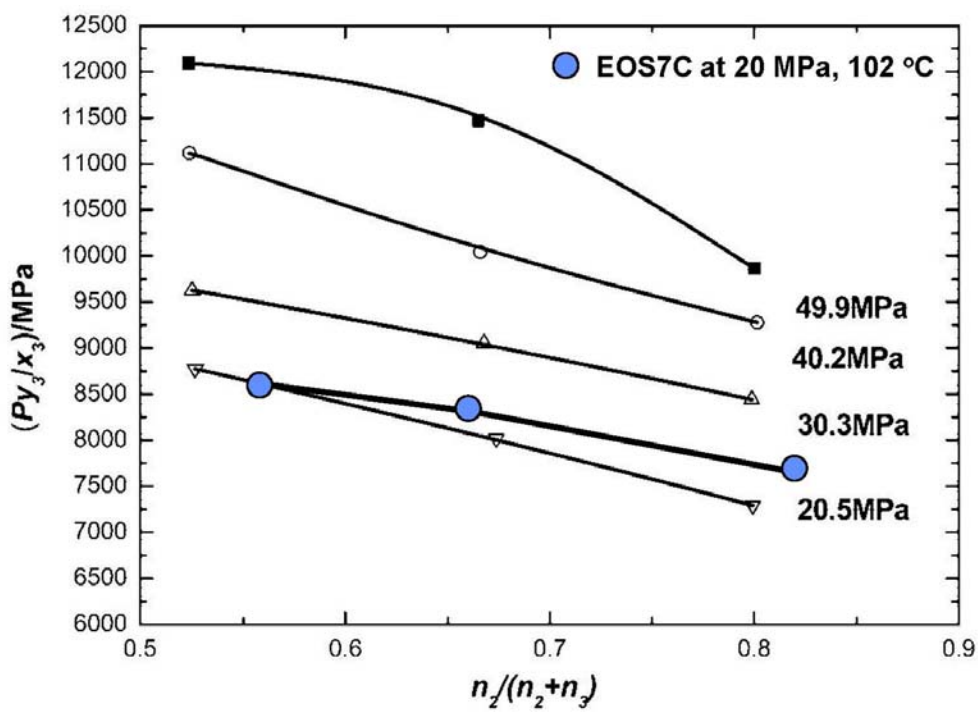

Figure 2. Results from Qin et al. (17) at T = 102 °C with EOS7C results for pure water (0 m NaCl) at 20 MPa superimposed showing reasonably good agreement. These results show that CH_4 (Component 3) solubility increases with higher CO_2 (Component 2) concentration in the water. EOS7C results assume the total mole fraction in the reaction cell ($n_2/(n_2+n_3)$) is

approximately equal to the mole fraction in the gas ($yn_2 = yCO_2$) a good approximation because the solubilities of CO_2 and CH_4 in water are relatively low.

We tested EOS7C at other pressure, temperature, and salinity conditions to further examine solubility trends in the multicomponent system H_2O-NaCl-CO_2-CH_4, with the expectation that the H_{CH4} trends shown in Figure 2 would not change, except for lower H_{CH4} values at lower pressures and higher H_{CH4} values at higher salinity (salting out). The results shown in Figures 3 and 4 confirm this expectation. As shown, H_{CH4} is much larger (lower solubility in the aqueous phase) for the 4 m brine (Figure 4) than for pure water at the same temperatures and pressures (Figure 3), and the trend remains toward lower H_{CH4} values at higher CO_2 concentration in the aqueous phase. From this testing, we conclude that the solubility model implemented into TOUGH2/EOS7C is appropriate for use in studying CH_4 exsolution in H_2O-NaCl-CO_2-CH_4 systems.

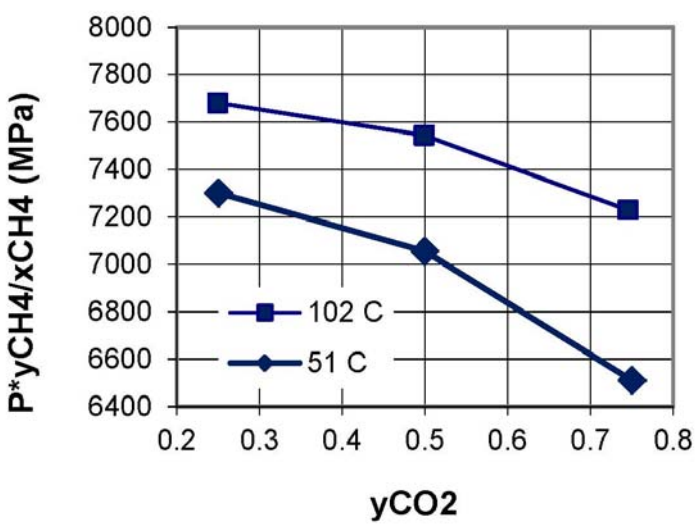

Figure 3. Effective Henry's Law coefficients computed with EOS7C for CO_2-CH_4 mixtures in pure water at 102 and 51 °C at 10 MPa.

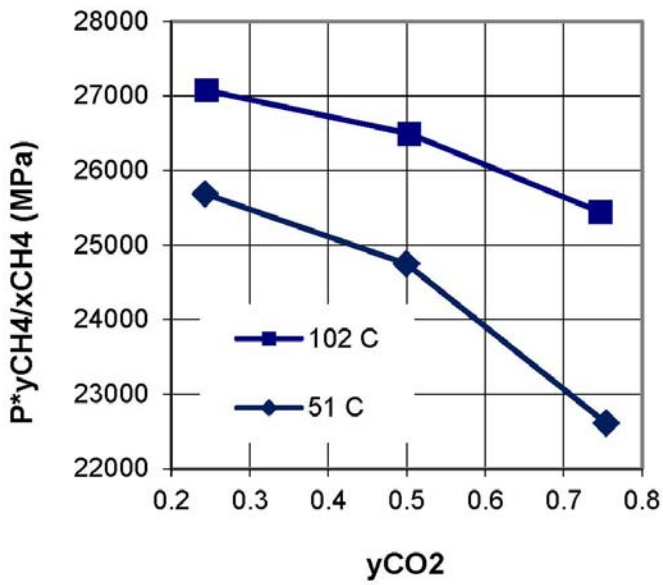

Figure 4. Effective Henry's Law coefficients computed with EOS7C for CO_2-CH_4 mixtures in a 4 m NaCl aqueous solution at 102 and 51 °C at 10 MPa.

Discussion of the CH_4 exsolution mechanism

One well-known example of the dissolution of one component affecting the solubility of a second component is the case of NaCl and CO_2 in water. When the salt concentration increases in the aqueous solution, the solubility of components such as CO_2 decreases. The process of gases coming out of solution (exsolving) as the salinity goes up is called the "salting out" effect, and is caused by the increase in ionic strength of the solution (from the dissociation of NaCl), which increases the effective concentration (activity) of dissolved gases, thus driving exsolution. One might expect a similar effect with the dissolution of other compounds in water. Specifically, one might expect dissolved CO_2 to diminish CH_4 solubility. However, exactly the opposite occurs. The measurements in (17) and the solubility model built into EOS7C both show the CH_4 solubility in the aqueous phase increases with the dissolution of CO_2 into the aqueous phase for a range of pressures and temperatures relevant for GCS (Figures 2-4).

Nevertheless, the result of adding dissolved CO_2 to a nearly saturated CH_4-water solution is the exsolution of a gas phase. The reason for this is that each gas species in the aqueous phase exerts partial pressure. When the sum of the partial pressures of all of the gas species exceeds the liquid pressure, a gas bubble forms. Technically, the formation of a gas bubble would require a pressure somewhat above the static liquid pressure to overcome surface tension effects (19), however, we ignore this effect here. Thus the appearance of gas bubbles in the aqueous phase is not an indication that CH_4 solubility goes down as CO_2 dissolves in water. It is simply that the sum of the partial pressures (i.e., the new total vapor pressure of the solution, see Dalton's Law) exceeds the liquid pressure.

The composition of a gas bubble exsolving from the aqueous phase is controlled by the Henry's Law coefficients of the various gas species and the concentrations of the gas components dissolved in the aqueous phase. Similarly, the composition of an aqueous phase at the boundary of a gaseous plume front is also controlled by the (effective) Henry's Law coefficients of the various gas species and the concentrations of the gas components in the gas phase.

Advection, diffusion, and dispersion are the mechanisms of transport in the fluid phases. These mechanisms control the length scales over which mixing in the aqueous and gas phases will occur during flow through porous media. In the simulations presented below, there is numerical dispersion which, depending on the grid discretization and numerical solution approach, can in some cases approximately mimic hydrodynamic dispersion. When free-phase CO_2 first invades a water-filled grid block containing CH_4 at near-saturation concentrations, a local equilibrium within the grid block is established that places a small amount of CO_2 into the CH_4-saturated water of the grid block as controlled by the total mass of CO_2 invading the grid block and by the Henry's Law coefficients. This results in an increase in the (total) gas pressure in the solution, which leads to exsolution of CH_4 into the gas phase. Because the solution is nearly at saturation with respect to CH_4, the gas phase becomes highly enriched in CH_4.

Verification of TOUGH2/EOS7C

The prior theory and modeling results of the injection of CO_2 into a one-dimensional horizontal column containing CH_4-saturated water have been presented (3). The main conclusion of that prior work was that CO_2 causes CH_4 exsolution, resulting in the generation of a gaseous CH_4

bank ahead of the CO_2 plume. The CH_4 bank was predicted to have very high CH_4 concentrations, but was of small volume, such that the predicted total flowing CH_4 amount was small.

Later, modeling results of injection of CO_2 into reservoirs with and without residual CH_4 gas were presented (11). These simulations also showed that CO_2 causes CH_4 exsolution resulting in the generation of a narrow CH_4 bank at the front of the CO_2 plume, but the focus was on relative permeability effects rather than gas exsolution. Here, we apply TOUGH2/EOS7C to the problem presented in (3) for code verification.

A sketch of Taggart's problem (3) is presented in Figure 5, and parameters of the problem are given in Table 1. In the problem, dry CO_2 is injected into a horizontal column that is initially fully liquid saturated and at (chemical) saturation with CH_4. The compositional outflow from the domain is quantified by the flowing mole fraction (qx^i), defined, for example, for i = CO_2, as

$$qx^{CO2} = \frac{q^{CO2}}{q^{CO2} + q^{CH4} + q^{H2O}} \qquad (2)$$

where the molar flows (q^i) are summed over both gas and aqueous phases. Results from TOUGH2/EOS7C and from (3) for this problem are shown in Figure 6. Figure 6a shows pressure, gas saturation, and mass fractions of CO_2 and CH_4 as a function of distance along the horizontal column at t = 3 days as simulated by TOUGH2/EOS7C. As shown in Figure 6a, the CO_2 displaces the CH_4-saturated water and produces a bank of gas with elevated CH_4 concentration at the gas-phase front at d = 42 m. The entry of two-phase mixture into previously single-phase aqueous grid blocks at the injection front is predicted to cause the gas phase to become predominately CH_4 as that small amount of CO_2 partitions between the aqueous and gas phases. Note that the maximum total mass fraction of CH_4 occurs just as the gas-phase saturation reaches zero. This is a critical aspect of this process relevant to questions about recovering CH_4 and about the CH_4 bank potentially interfering with efforts to image the injected CO_2 plume. In simulations not shown here, we determined that increasing the residual gas (physical) saturation

S_{gr} (aka S_{crit}) causes a delay in the arrival of the CH_4 bank due to the additional time it takes for the gas (physical) saturation to become high enough to allow gas-phase mobility, but does not otherwise affect the results. Figures 6b and 6c display the flowing mole fractions of CO_2, CH_4, and H_2O at the outlet of the model computed with TOUGH2/EOS7C and as shown in (3), and demonstrate good agreement between the two. The main processes displayed in this 1D problem are water displacement, CO_2 invasion, and partitioning of CO_2 and CH_4 between gas and aqueous phases.

Table 1. Properties of the 1D displacement problem after Taggart (2009).

Property	Value
Porosity (ϕ)	0.25
Permeability (k)	1.0×10^{-12} m^2
Capillary Pressure (P_{cap})	0.0
Relative Permeability (k_r)	power-law k_{rl} and k_{rg} with power = 2, S_{lr} = 0.15, S_{gr} = 0
Pressure (initial and right-hand side boundary condition)	2.04×10^7 Pa (3000 psi)
Temperature (isothermal)	91.8 °C (197.2 °F)
CO_2 injection rate	9.4×10^{-4} kg/s (1 res. Bbl/day)
Initial aqueous phase saturation	S_l = 1.0
Grid spacing	0.5 m

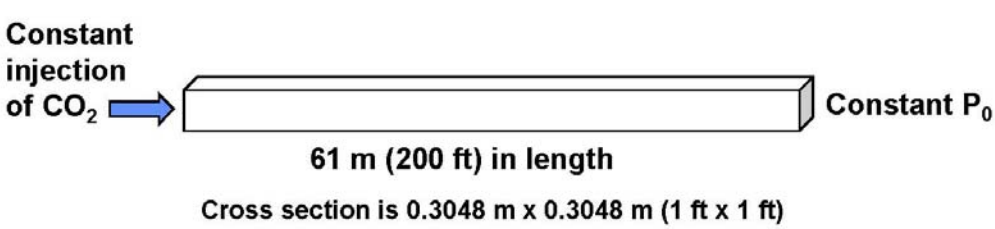

Figure 5. Sketch of 1D model flow domain after (3).

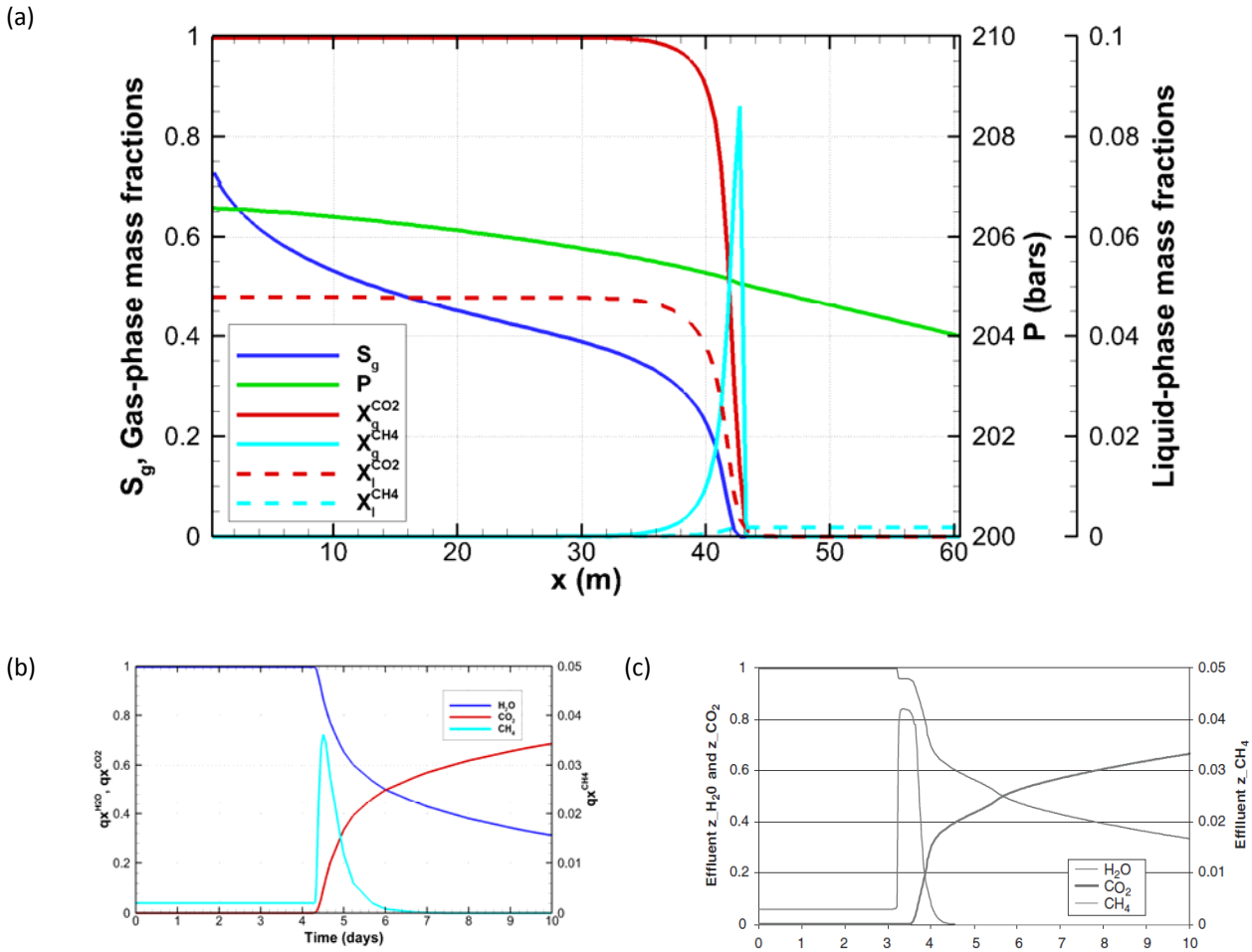

Figure 6. (a) TOUGH2/EOS7C simulation results at t = 3 days as a function of distance from the inlet. (b) TOUGH2/EOS7C simulation results of flowing mole fractions (qx^{H2O}, qx^{CO2}, qx^{CH4}) at the outlet for power-law k_{rl} and k_{rg} with power = 2. Note the sharp peak in the CH_4 profile, consistent with (c) prior results (3).

Numerical dispersion

Because CH_4 exsolution due to CO_2 injection relies on CO_2 invasion into the CH_4-rich waters at the phase front, and such advection is enhanced by numerical dispersion in discretized numerical models, we undertook an investigation of the effects of numerical dispersion. Numerical dispersivity in this 1D problem with upstream weighting in TOUGH2 is equal to one-half the grid spacing multiplied by the Darcy velocity (ΔY/2 * v) (e.g., (20) p. 238). To investigate the effects of numerical dispersion, we carried out simulations of the 1D test problem with three

different grids, coarse (15 grid blocks in the Y-direction), medium (60 grid blocks in the Y-direction), and fine (240 grid blocks in the Y-direction). As shown in Figure 7, numerical dispersion does influence the results. Specifically, the coarser gridding causes greater width of the CH_4 front, and the faster propagation of the injected CO_2. Numerical dispersion also affects the peak CH_4 concentration in the CH_4 bank, but these changes are not completely systematic with grid refinement as seen in Figure 7. By t = 3 days, it seems that the trend is apparent that coarser gridding causes a wider CH_4 bank with lower peak concentration and finer gridding causes a narrower CH_4 bank with higher peak concentration. In addition, the peak concentration of the CH_4 bank tends to grow with time over the three days and 60 m length of the system.

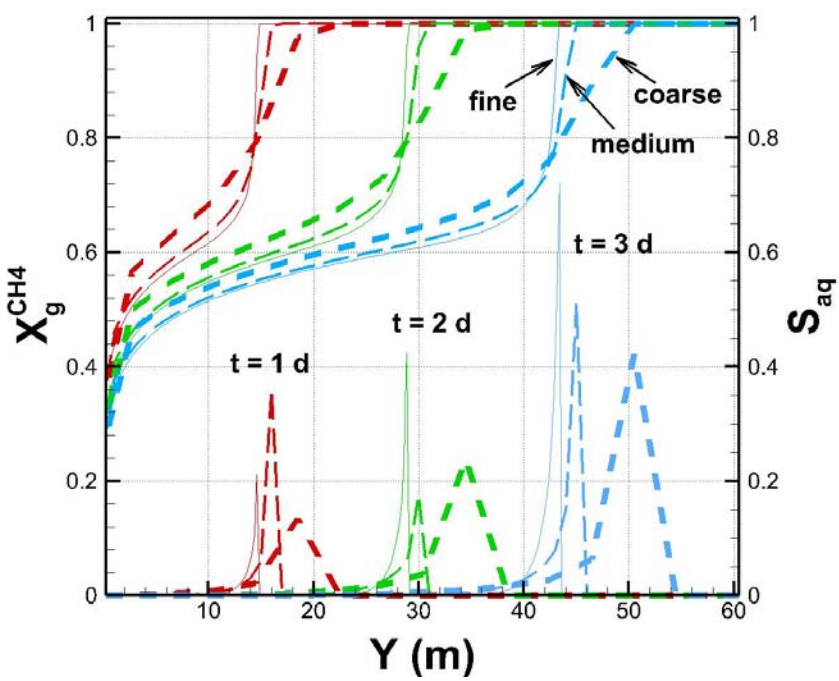

Figure 7. Simulation results for the 1D model problem showing evolution of the peak concentration and width of the CH_4 bank as a function of grid resolution where fine corresponds to ΔY= 0.25 m (240 grid blocks), medium to ΔY= 1 m (60 grid blocks), and coarse to ΔY = 4 m (15 grid blocks).

To investigate the growth in intensity of the CH_4 bank over time, we lengthened the 1D problem from 60 m to 240 m while keeping the same grid size as the fine grid (ΔY= 0.25 m). As shown in Figure 8, the peak concentration of the CH_4 bank grows until about 12 days and then stabilizes with nearly pure CH_4 in the bank. The width of the CH_4 bank continues to grow, as more CH_4 is continually exsolved as the bank moves along. Note that this CH_4 bank occurs mostly within a region where the aqueous phase saturation is increasing rapidly to one. The overall conclusion here is that simulation results are affected by numerical dispersion, but the effects are generally predictable in this 1D problem, with higher resolution models producing sharper CH_4 banks with higher CH_4 concentration within the bank.

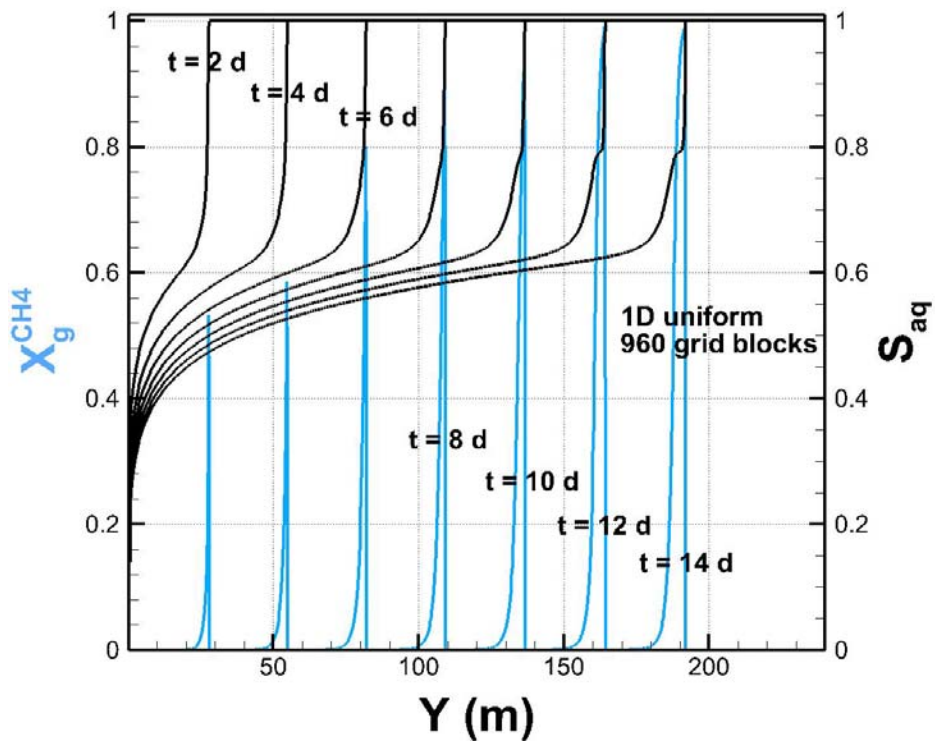

Figure 8. Simulation results for an extended 1D model problem (240 m in length) for a fine grid (ΔY = 0.25 m) showing the peak X_g^{CH4} increases with time as does the width of the CH_4 bank.

Because our 2D simulations (next section) are in a radial system, we also investigated the width and intensity of the CH_4 bank for the 1D system but with a radial geometry. In the radial system, the width of the CH_4 bank seems to stabilize after about 4 days (bank volume continues to grow because of the radial geometry), while the peak concentration is still changing at 14 days as shown in Figure 9.

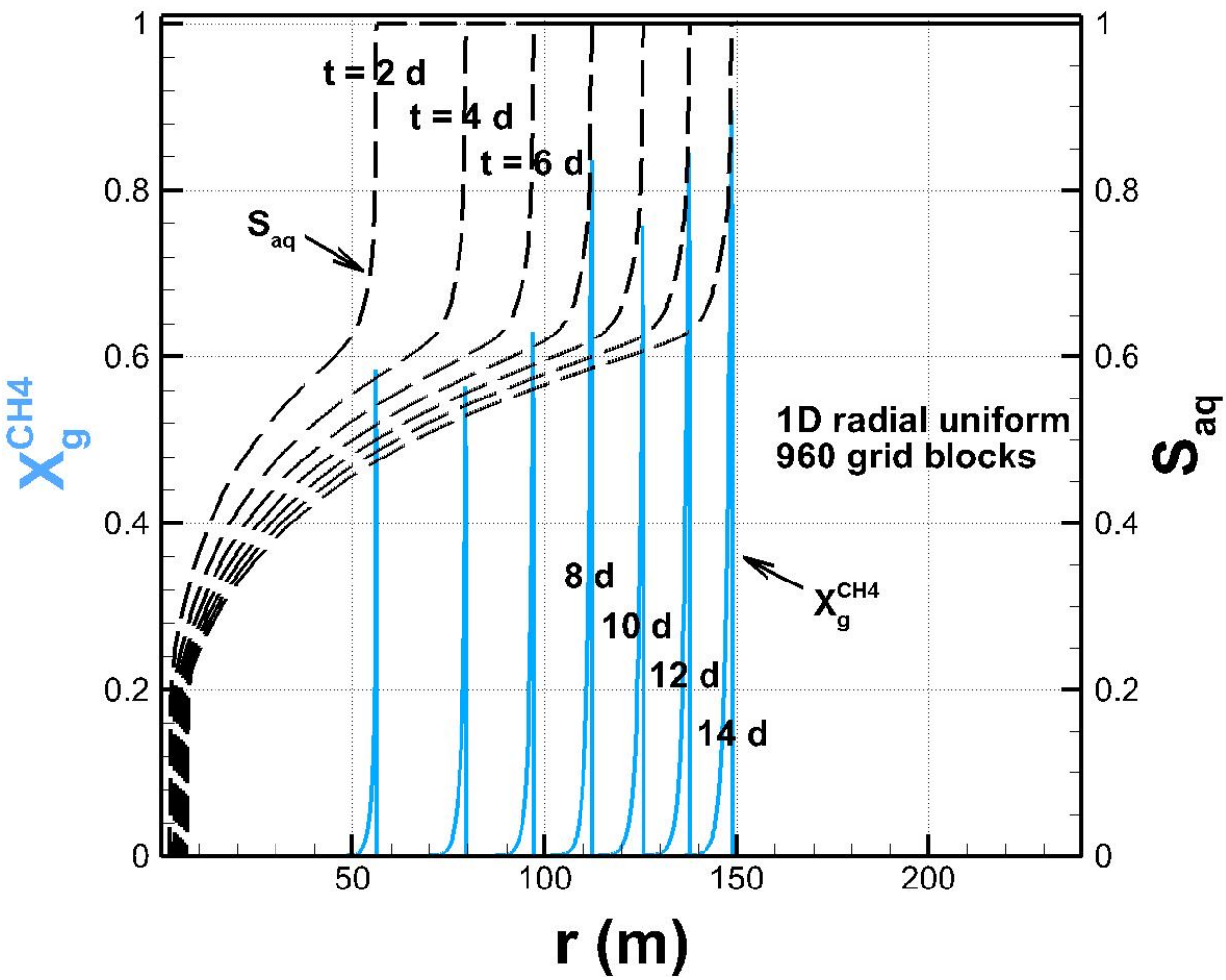

Figure 9. Simulation results for a 1D radial grid showing small changes in peak concentration and width of the CH_4 bank due to the geometric effect of the radial grid.

Simulation of 2D radial model system

Model Properties

In order to understand and evaluate the extent and implications of CH_4 exsolution induced by CO_2 injection for large-scale CO_2 injection projects, we carried out TOUGH2/EOS7C (22, 7) simulations of CO_2 injection into an idealized 2D radial system. The properties of the model system were chosen to include features of interest such as multiple layers with different permeability, including a low-permeability layer (baffle) with potential for structurally trapping exsolved CH_4. The main features of the system include zero dip, fresh water, isothermal conditions, constant isotropic permeability within each layer, uniform porosity, capillary pressure strength proportional to the inverse square root of permeability (i.e., Leverett scaling), a multilayer CO_2 injection rate set to be proportional to the permeability-thickness product of each layer at a rate of 14 kg/s (0.44 Mt CO_2/yr). Injection lasts for 40 years. Details of the system properties are presented in Table 2.

The domain discretization and layering are shown in Figure 10. The gradually changing grid-block size in the radial direction was chosen to resolve flow features near the well (where grid block width is 1 m), and economize on simulation time at greater distances. Note the domain is 10 km in radius to avoid strong influence of the outer boundary. The model is 400 m thick and contains 40 layers, each 10 m thick. Given the properties of the formations and the assumed injection interval, most of the injected CO_2 is expected to flow into Layers 2 and 3 (the most permeable units). With the assumed properties and configuration, including a continuous shale layer (Layer 4), it is expected that buoyant CO_2 and/or exsolved CH_4 will accumulate for some period under the shale in the model system.

The initial conditions for all simulations have hydrostatic pressure (thus no horizontal pressure gradient) and constant temperature (104 ^{o}C). The top and bottom boundaries are closed to flow, while the outer (right-hand side) boundary is held at a constant hydrostatic pressure. In the first set of simulations, we assumed fully saturated initial conditions in the model with water containing dissolved CH_4 just below the concentration at which CH_4 bubbles would form (i.e., just below chemical saturation). In the second set of simulations, initial conditions with residual

CH_4 were produced by running a preliminary simulation with a small amount of gaseous CH_4 to a gravity equilibrium, to examine the effect of initial residual gas.

Table 2. Properties of the simplified single-well radial case study.

Property	Value
Porosity (ϕ)	0.15
Dip	0 degrees
Pressure at top of domain (initial)	2.24×10^{7} Pa
Temperature (isothermal)	104 °C
Permeability (k) Reservoir Layer 1 Reservoir Layer 2 Reservoir Layer 3 Shale Layer 4 Reservoir Layer 5	 1.0×10^{-14} m^2 5.0×10^{-14} m^2 2.5×10^{-14} m^2 1.0×10^{-15} or 1.0×10^{-16} m^2 2.5×10^{-14} m^2
Capillary Pressure (P_{cap}) and Relative Permeability (k_r) *Terminology:* λ = m = 1-1/n = power in expressions for P_{cap} S_{lr} = aqueous-phase residual saturation S_{gr}= gas-phase residual saturation $P_{c0} = \alpha^{-1}$ = capillary pressure strength between aqueous and gas phase P_{cmax} = maximum possible value of P_{cap}	van Genuchten (22) capillary pressure and relative permeability for liquid, Corey (23) relative permeability for gas $\lambda = 0.40$ $S_{lr} = 0.27$ $S_{gr} = 0.01$ P_{c0} = 1190 Pa (for Layer 2) $P_{cmax} = 1 \times 10^{8}$ Pa
Single-well injection rate of 0.44 Mt/yr for 40 years[1].	14 kg/s

[1]M = million

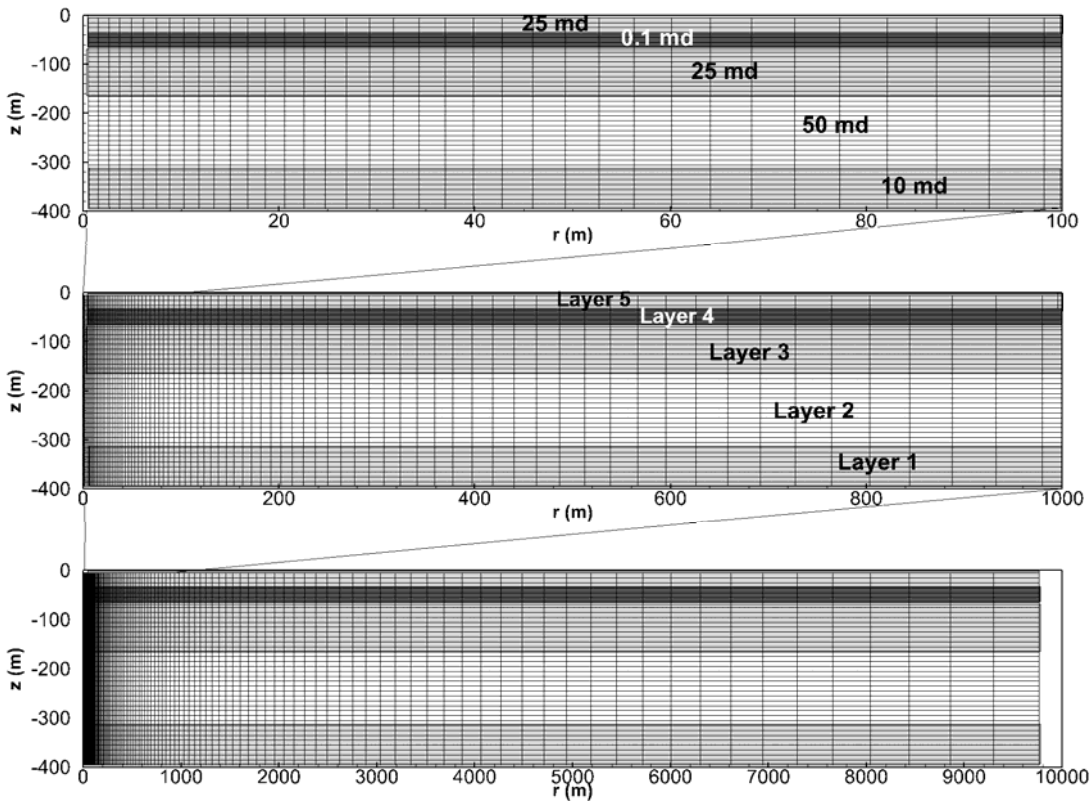

Figure 10. Refined discretization showing gradual increase of grid block width throughout the radial extent of the domain, and uniform spacing in the vertical direction. Top two plots are successive blow-ups of the bottom plot near the injection well (left side).

Results

Case 1: Dissolved CH_4

Figures 11-13 show results for the case of CH_4 dissolved initially in the water (no residual gas). As expected, injection of CO_2 into CH_4-saturated water results in the exsolution of CH_4 at the leading edge of the CO_2 plume. While the concentration of CH_4 in the gas at the leading edge is very high (nearly 100%), the amount of gas there is very small ($S_g < 0.1$). Buoyancy forces on the lighter CH_4 gas result in strong upward movement of the bank of CH_4, which is barely apparent at 100 days (Figure 11), and dominant at later times (Figures 12-13). The blob-like nature of the CH_4 bank seen in Figures 12-13 is a numerical artifact, caused by the rectangular grid's poor representation of the sloping bank. Exsolved CH_4 accumulates under the shale layer for a time (Figures 11-12), but eventually moves through it to accumulate at the top of the model

domain (Figure 13). The sweep of CO_2 effectively strips all of the CH_4 from the aqueous phase within the region of the CO_2 plume. The gas concentrations in the CO_2-swept region are dominated by the CO_2 that is injected.

As shown in Figure 11 the shale limits the flow of injected buoyant CO_2 upward, creating a strong pressure gradient across this formation. Gas saturations reach about 30%, and the vast majority of the gas-phase plume is filled with nearly pure CO_2. By a time of five years (Figure 12), there is enhanced spreading under the shale where gas saturation is higher due to accumulation of CO_2. Also, by five years the gas saturation becomes very high near the well, due to dry-out of the formation as residual-phase water evaporates into the gas phase. The 40-year results (Figure 13) indicate that enhanced spreading under the shale persists, even as near the well some gas flows upward through the shale. The gas saturation distribution in Figure 13 shows that S_g remains notably lower in the shale than in the underlying sand, due to a combination of the shale's lower permeability and higher capillary pressure strength.

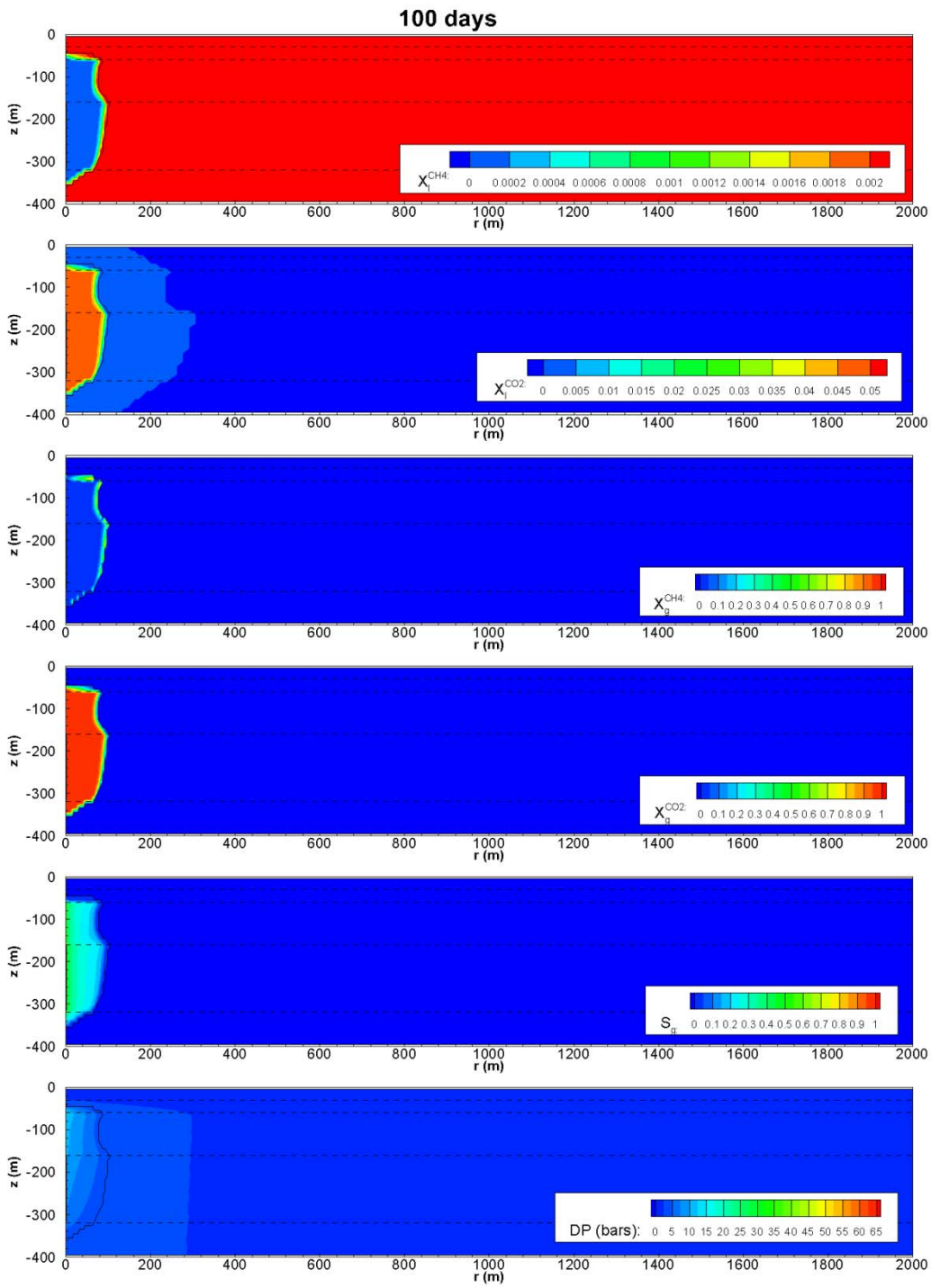

Figure 11. Results at t = 100 days of mass fraction CH_4 in the aqueous phase (X_l^{CH4}), mass fraction CO_2 in the aqueous phase (X_l^{CO2}), mass fraction CH_4 in the gas phase (X_g^{CH4}), mass fraction CO_2 in the gas phase (X_g^{CO2}), gas saturation (Sg) and pressure change (DP). The dashed lines identify the model layering. The CH_4 exsolution bank is clearly visible as the maximum

X_g^{CH4} just inside of the boundary of the gas-phase plume. The single solid black contour line most easily seen in the last frame is the $S_g = 1 \times 10^{-5}$ isopleth, showing the extent of the gas-phase in the domain.

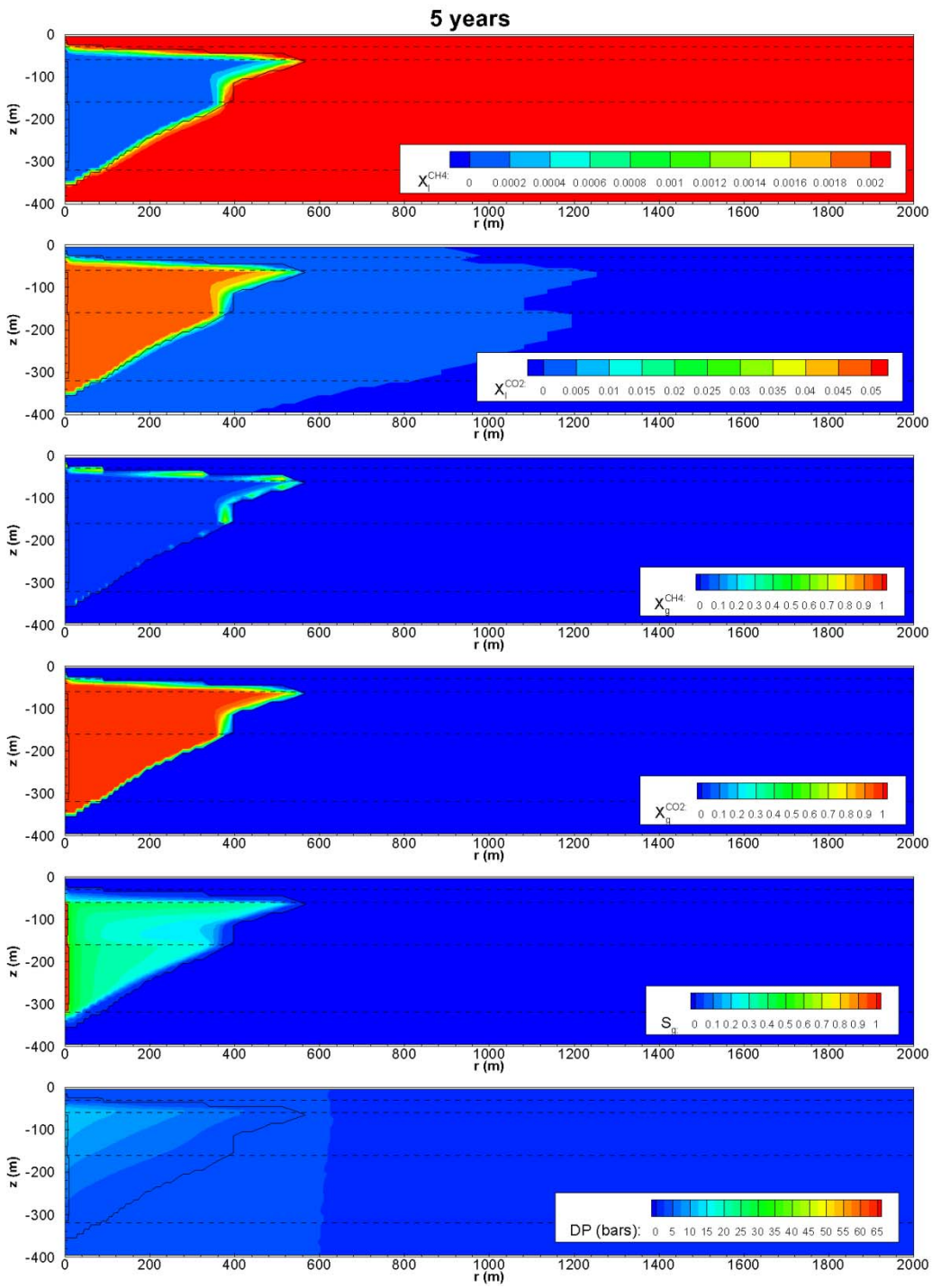

Figure 12. Results at t = 5 years of mass fraction CH_4 in the aqueous phase (X_l^{CH4}), mass fraction CO_2 in the aqueous phase (X_l^{CO2}), mass fraction CH_4 in the gas phase (X_g^{CH4}), mass fraction CO_2 in the gas phase (X_g^{CO2}), gas saturation (S_g) and pressure change (DP). The dashed lines identify the model layering. Note the CH_4 exsolution bank extends through the shale. The single solid

black contour line most easily seen in the last frame is the S_g = 1 x 10^{-5} isopleth, showing the extent of the gas-phase in the domain.

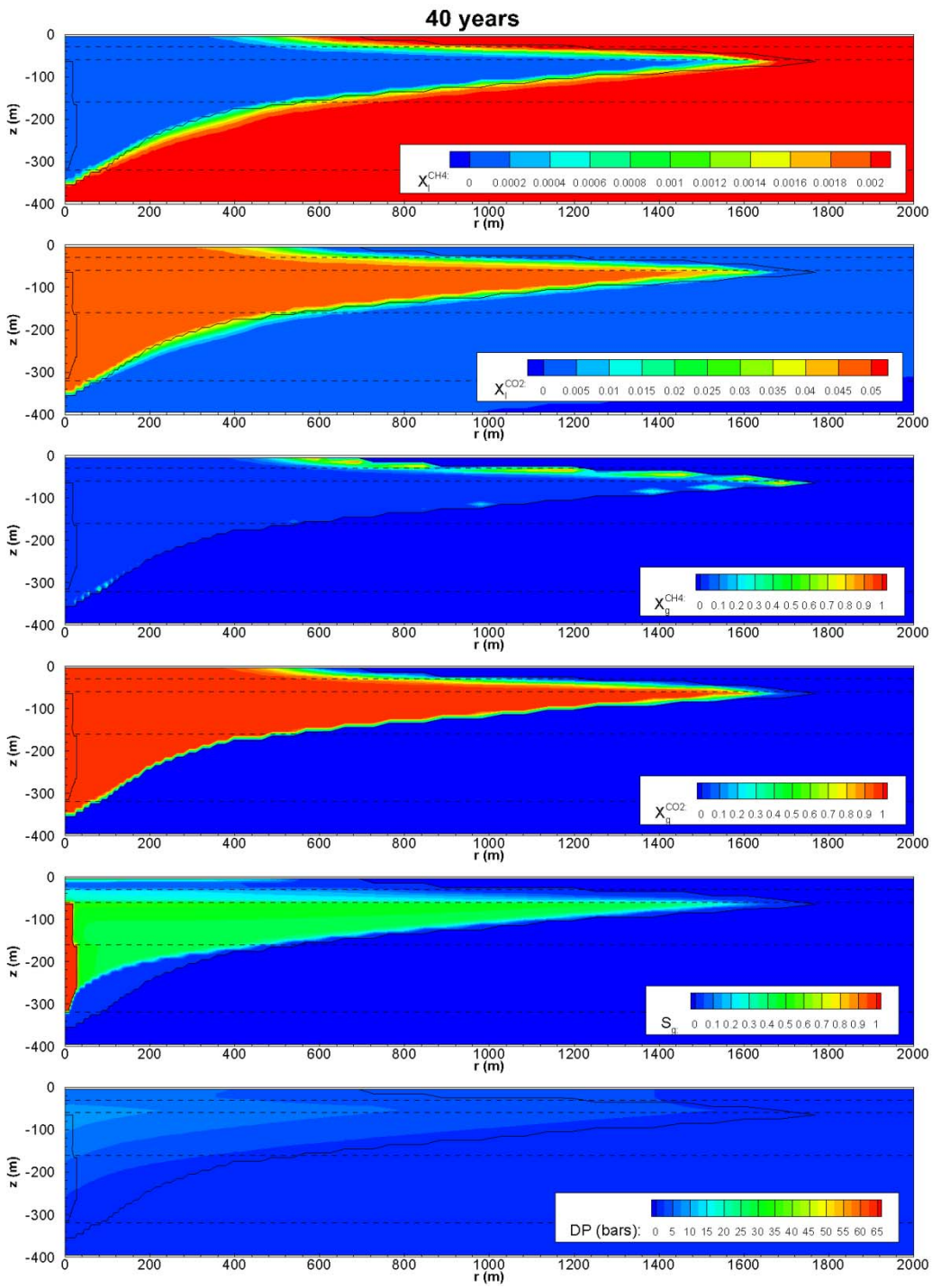

Figure 13. Results at t = 40 years of mass fraction CH_4 in the aqueous phase (X_l^{CH4}), mass fraction CO_2 in the aqueous phase (X_l^{CO2}), mass fraction CH_4 in the gas phase (X_g^{CH4}), mass fraction CO_2 in the gas phase (X_g^{CO2}), gas saturation (S_g) and pressure change (DP). The dashed lines identify the model layering. Exsolved CH_4 is spread out in the shale and Layer 5, but only

in regions with very small gas saturation. The single solid black contour line most easily seen in the last frame is the $S_g = 1 \times 10^{-5}$ isopleth showing the extent of the gas-phase in the domain.

Case 2: Initial residual CH_4 gas

In Case 2, we investigated the effect of injection of CO_2 into a system with residual gas, similar to our previous work (11), but with emphasis on CH_4 exsolution rather than relative permeability and injectivity. We establish initial conditions with residual CH_4 gas by specifying a constant saturation of $S_g = 0.26$, then letting the system evolve for 1000 years. This results in a slight stratification, with the saturation distribution shown in Figure 14. Gas with $S_g > S_{gr}$ is slightly mobile. The value of residual gas saturation is $S_{gr} = 0.27$.

Results for Case 2 are shown in Figures 15-17. Because residual CH_4 gas was present everywhere initially, the composition of the gas-phase near the leading edge of the CO_2 plume is nearly pure CH_4, which means the generation of a CH_4 front does not show up as a distinct bank because all of the existing gas away from the CO_2 plume is pure CH_4. Nevertheless, the tendency for exsolution to occur is still present as CO_2 dissolves into the aqueous phase. As was observed in (11), the main effect of the presence of residual gas is to restrict the flow of water (aqueous phase) through relative permeability effects such that the pressure rise (*DP*) for a given CO_2 injection rate is much higher than when residual gas is not present. This can be seen by comparing *DP* in Figures 11 and 15. As for the growth and evolution of the CO_2 plume, at early time (100 days), the systems with zero residual gas and with residual gas are similar (Figures 11 and 15), but by $t = 5$ years, significant differences arise as relative permeability effects play out (Figures 12 and 16). The larger pressure gradients required to drive flow when residual gas is present make buoyancy flow relatively less important, resulting in much less upward flow of the CO_2 plume. Figure 16 shows that the extent of the CO_2 plume in each layer is roughly proportional to layer permeability, with just a small accumulation under the shale layer. By 40 years, however, buoyancy flow again dominates (Figures 13 and 17), with strong upward gas-phase flow and extensive spreading under the shale layer. In fact, the radial extent of the CO_2 plume is greater for the case with residual CH_4 present. Near the well, Figure 17 shows that while mobile gas phase has moved through the shale all the way to the top of the formation, the composition of the gas above the shale is mainly CH_4, and saturation remains significantly lower than below the shale.

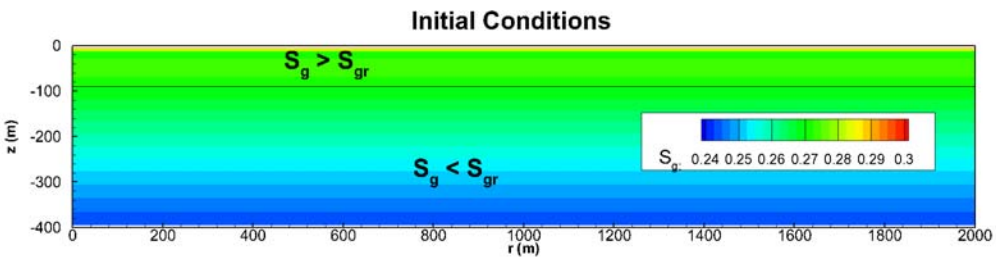

Figure 14. Initial distribution of residual CH_4 gas along with the $S_g = S_{gr} = 0.27$ isopleth (black line).

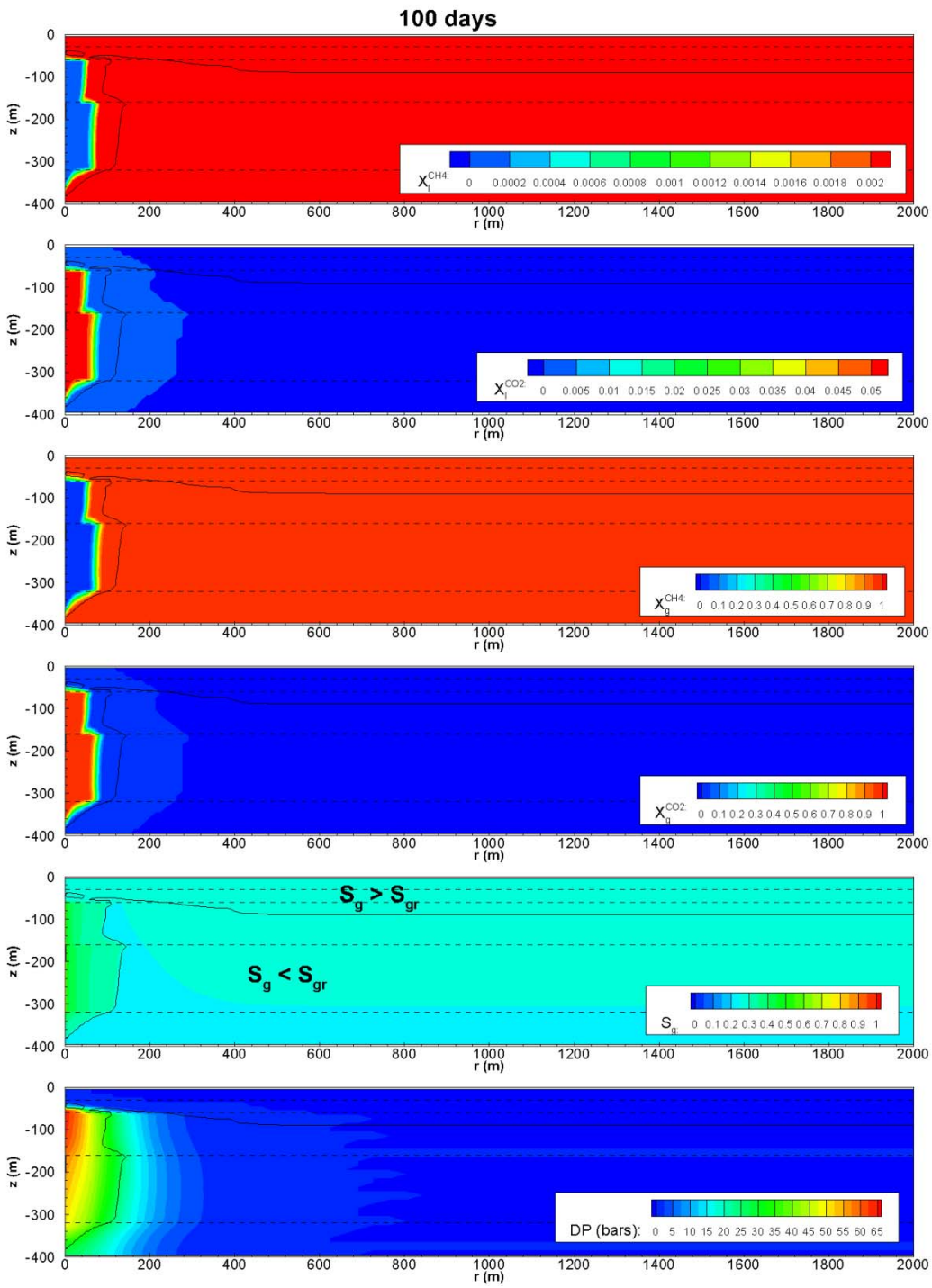

Figure 15. Results at t = 100 days of mass fraction CH_4 in the aqueous phase (X_l^{CH4}), mass fraction CO_2 in the aqueous phase (X_l^{CO2}), mass fraction CH_4 in the gas phase (X_g^{CH4}), mass fraction CO_2 in the gas phase (X_g^{CO2}), gas saturation (S_g) and pressure change (DP). The single

solid black contour line is the S_g = 0.27 isopleth, showing the extent of the residual gas-phase that is present throughout the domain. The dashed lines identify the model layering.

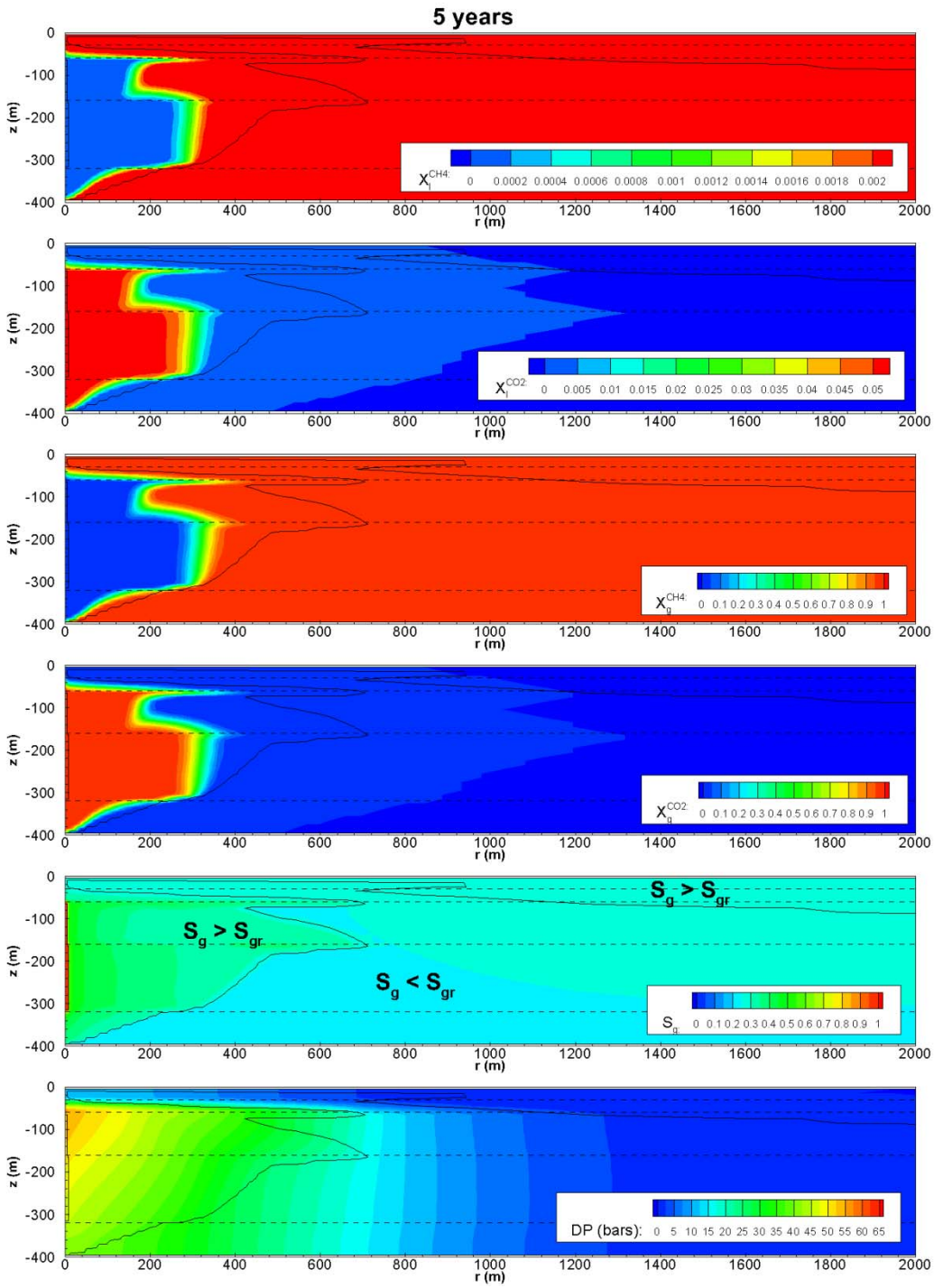

Figure 16. Results at t = 5 years of mass fraction CH_4 in the aqueous phase (X_l^{CH4}), mass fraction CO_2 in the aqueous phase (X_l^{CO2}), mass fraction CH_4 in the gas phase (X_g^{CH4}), mass fraction CO_2

in the gas phase (X_g^{CO2}), gas saturation (S_g) and pressure change (DP). The single solid black contour line is the S_g = 0.27 isopleth, showing the extent of the residual gas-phase that is present throughout the domain. The dashed lines identify the model layering.

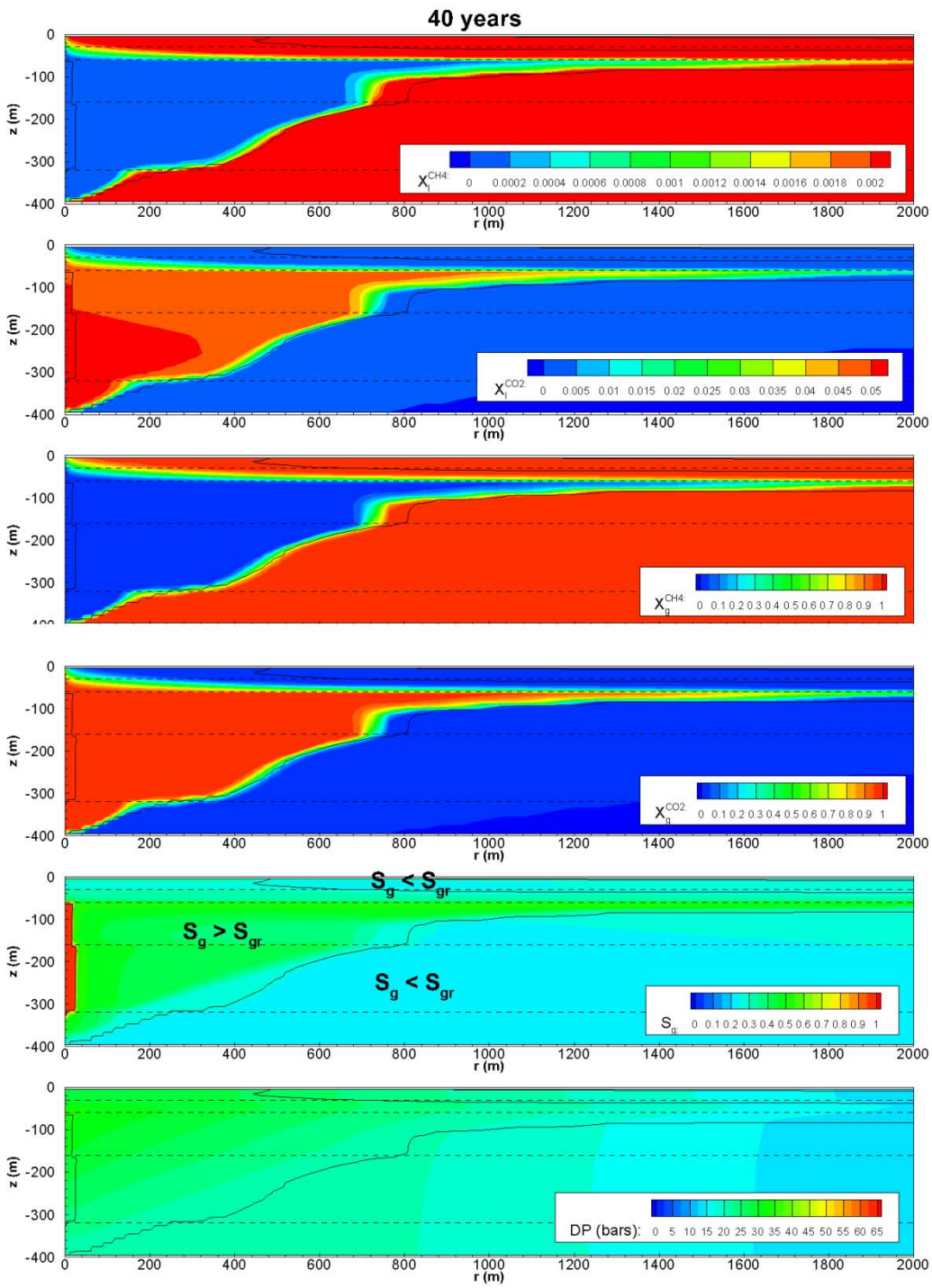

Figure 17. Results at t = 40 years of mass fraction CH_4 in the aqueous phase (X_l^{CH4}), mass fraction CO_2 in the aqueous phase (X_l^{CO2}), mass fraction CH_4 in the gas phase (X_g^{CH4}), mass fraction CO_2 in the gas phase (X_g^{CO2}), gas saturation (S_g) and pressure change (DP). The single

solid black contour line is the S_g = 0.27 isopleth, showing the extent of the residual gas-phase that is present throughout the domain. The dashed lines identify the model layering.

Long-term post-injection results are shown in Figures 18 and 19. Figure 18 shows that gas saturation steadily decreases towards S_{gr}, and that the shale layer continues to provide a barrier to buoyancy flow. The dry-out region around the well shrinks until it has disappeared by 500 years. Figure 19 shows that the mass fraction of CO_2 within the gas-phase plume is not changing much. In a system with a dipping formation or regional flow, there would be an opportunity for the CO_2 plume to come into contact with brine not already saturated with dissolved CO_2, so the plume would gradually disappear as CO_2 dissolved. Similarly, if brine not already saturated with dissolved CH_4 entered the system, the residual CH_4 could dissolve as well.

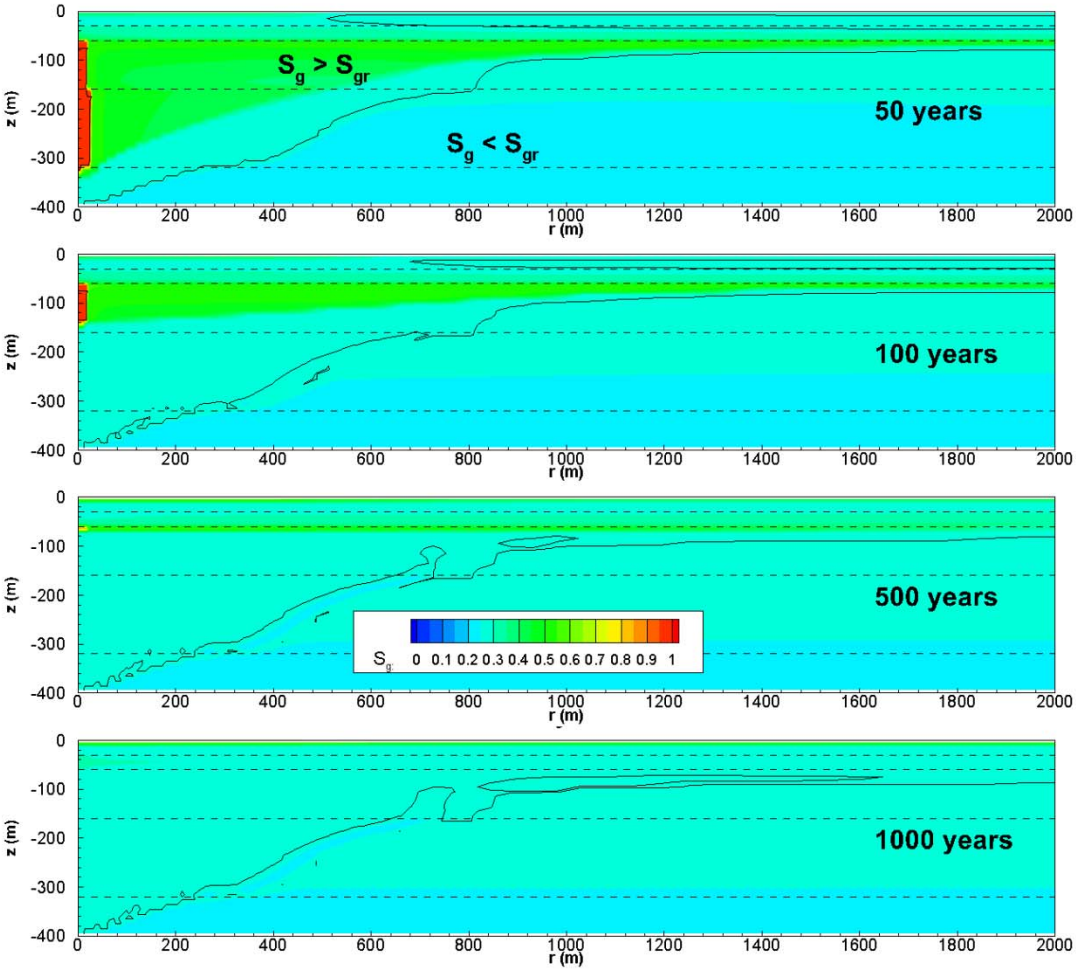

Figure 18. Long-term post-injection results of gas saturation (color contours) and S_g = 0.27 isopleth. The dashed lines identify the model layering. The baffle effect of the shale remains as higher gas saturations are observed under it.

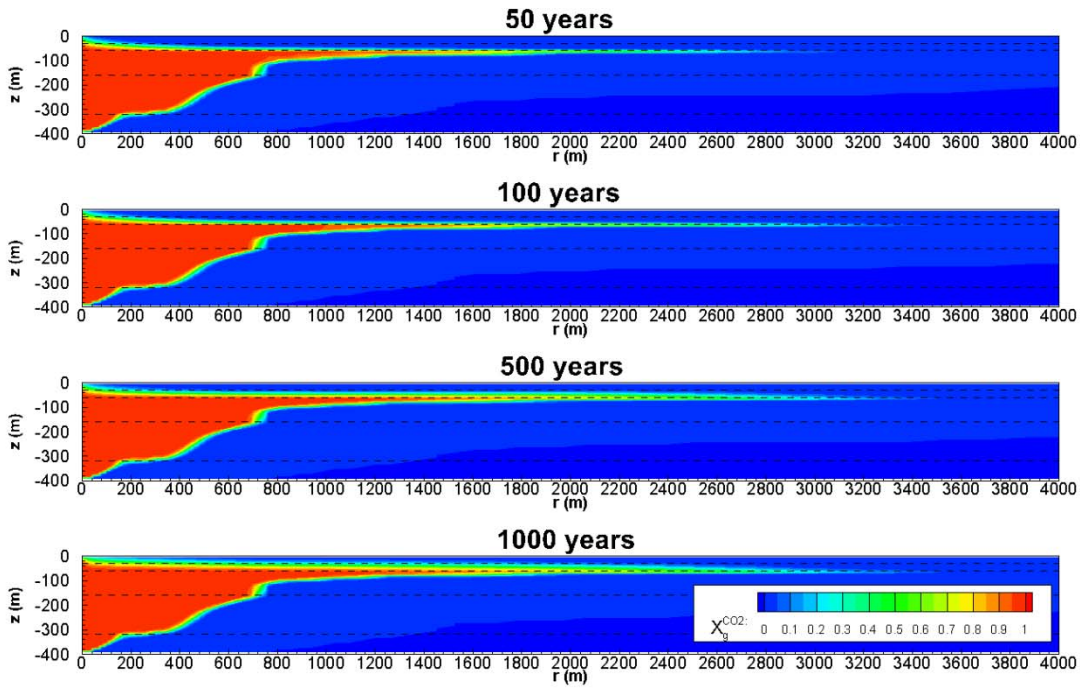

Figure 19. Long-term post-injection results of mass fraction CO_2 in the gas phase (X_g^{CO2}) showing very small changes after 100 years.

Summary of 2D radial simulations

A CH_4 bank forms at the leading edge of CO_2 injected into water containing dissolved CH_4. The CH_4 bank occurs in a region of very small gas saturation. The CH_4 bank tends to rise upward by the buoyancy effect. For the case of residual CH_4 gas present initially, the pressure rise due to injection is larger, all other things being equal, due to decreased relative permeability of the formation to the water (aqueous phase) as observed in previous 1D simulations (11). In the 2D case study shown here, we also observe that buoyancy flow is less when there is residual gas present, presumably because the density contrast between injected CO_2 and the water-CH_4 gas mixture is smaller, and because the buoyancy force is smaller compared with the advective pressure increase. With less buoyancy flow, there is diminished flow upward through the shale, and greater radial extent of the CO_2 plume. For the post-injection period out to hundreds of years, there is very little movement of the CO_2 plume. Over time, the gas saturation gradually decreases to nearly the residual gas saturation as CO_2 continues to dissolve and diffuse into the aqueous phase.

Summary

The solubility model of TOUGH2/EOS7C agrees with laboratory measurements (17) which show that CH_4 solubility actually increases with dissolved CO_2 content. But the partial pressure exerted by dissolved CO_2 in water with CH_4 dissolved at near-saturation values causes the formation of a CH_4-rich gas phase despite the increase in CH_4 solubility.

TOUGH2/EOS7C has been verified against another numerical solution (3) on a 1D horizontal CO_2 injection problem. Numerical dispersion causes a wider and lower concentration CH_4 bank, but the CH_4 bank strength levels off when the grid resolution is fine enough.

Numerical experiments in a 2D model system show the formation of the CH_4 bank and its tendency to migrate upwards. But as in the 1D problem, the nearly pure CH_4 bank occurs in a region with very small gas saturation, meaning the amount of CH_4 is modest and what is present is not very mobile.

Implications for geologic carbon sequestration

The interference of CH_4 exsolution on seismic monitoring of CO_2 injection does not appear to be a concern. First, the gas saturation in the CH_4-rich leading-edge region is very small, and second, the CH_4 bank is adjacent to the CO_2 phase front. Granted the p-wave velocity is very sensitive to gas saturation at small values of gas saturation, but the detection of gas (e.g., CH_4 or super-critical CO_2) at this location would indicate the region of the CO_2 plume anyway because the CH_4 bank is located at the leading edge of the CO_2 plume. While we are not aware of ways to distinguish between CO_2 and CH_4 by surface seismic methods, modeling of the details of the geophysical response of CH_4 adjacent to CO_2 could be carried out as a way to investigate whether CO_2 and CH_4 gas regions could be resolved by seismic monitoring.

Regarding the possibility of substantial increase in pressure that could occur due to CH_4 diluting supercritical CO_2, this does not appear to be likely. The reason is that the exsolution occurs at the edge of the CO_2 plume, and the main CO_2 plume tends to push CH_4 out to the periphery of the plume. The main plume remains nearly pure CO_2 through its overwhelming ability to dilute trailing edge CH_4.

As for the effect on injection arising from relative permeability effects of an exsolving CH_4-rich gas phase, the saturations are very small and this does not seem to be a big factor in the simulations. This result is also relevant to the question of whether CH_4 could be produced for beneficial use from an artificially created CH_4 bank. In short, the feasibility appears low because the gas-phase saturations are too small. The simulations show that any region of high gas saturation is dominated by CO_2. We note that our simulations assumed a fresh water (zero salinity) which allowed even more dissolved CH_4 to exist than would exist in an actual saline brine, and still we found the amounts of CH_4 exsolved to be too small in the general case to create obvious accumulations that could strongly impact GCS or be available for commercial exploitation. Although not investigated here, we can speculate that engineered heterogeneity through hydraulic fracturing and/or less regular and more creative injection and fluid manipulation schemes could conceivably be developed to optimize CH_4 exsolution and accumulation for potential beneficial extraction.

In summary, our simulations suggest that dissolved CH_4 in formation waters produces some interesting exsolution effects, but dissolved CH_4 and its exsolution do not appear to have serious

implications for geologic carbon sequestration. This conclusion is based on our experiences with the simulations presented here that make use of relatively homogeneous systems and a simple injection process as envisioned for geologic carbon sequestration.

Acknowledgment

We thank two anonymous reviewers for helpful comments that allowed us to refine the presentation. Support for this work was provided by Chevron with project management and guidance from Scott Imbus (Chevron). Additional support was provided by the Assistant Secretary for Fossil Energy (DOE), Office of Coal and Power Systems, through the National Energy Technology Laboratory (NETL), and by Lawrence Berkeley National Laboratory under Department of Energy Contract No. DE-AC02-05CH11231.

References

1. Doherty MG, Randolph PL, Rogers LA and Poonawala NA, Methane production from geopressured aquifers. J Petrol Geol. 1982;34(7):1591-1599.

2. Metz B, Davidson O, de Coninck H, Loos M, Meyer L. IPCC, 2005: IPCC special report on carbon dioxide capture and storage. Prepared by Working Group III of the Intergovernmental Panel on Climate Change. Cambridge, United Kingdom and New York, NY, USA; 2005;442 pp.

3. Taggart I. Extraction of dissolved methane in brines by CO_2 injection: Implication for CO_2 sequestration. Soc. Pet. Eng. 2009;SPE-12460.

4. Reamer HH, Olds RH, Sage BH, Lacey WN. Methane-carbon dioxide system in the gaseous region. Ind. Eng. Chem. 1944;36:88-90.

5. Oldenburg CM, Webb SW, Pruess K, Moridis GJ. Mixing of stably stratified gases in subsurface reservoirs: a comparison of diffusion models. Trans. Porous Med. 2004;54(3):323–334.

6. Carcione JM, Picotti S, Gei D, Rossi G. Physics and seismic modeling for monitoring CO_2 storage. Pure Appl Geophys. 2006;163.1:175-207.

7. Oldenburg CM, Moridis GJ, Spycher N, Pruess K. EOS7C Version 1.0: TOUGH$_2$ module for carbon dioxide or nitrogen in natural gas (methane) reservoirs. Lawrence Berkeley National Laboratory Report. March 2004; LBNL-56589.

8. Buckley SE, Hocott CR, Taggart Jr MS. Distribution of dissolved hydrocarbons in subsurface waters. Habitat of oil: Am Assoc Petr Geol B. 1958:850-882.

9. Bebout DG, Weise BR, Gregory AR, Edwards MB. Wilcox sandstone reservoirs in the deep subsurface along the Texas Gulf Coast: University of Texas, Austin, Bureau of Economic Geology. Report of Investigations. 1982; 117.

10. Bryant SL, Pope GA. Storing Carbon Dioxide and Producing Methane and Geothermal Energy from Deep Saline Aquifers. U.S. Patent Application 13/208,854, filed August 12, 2011.

11. Oldenburg CM, Doughty C. Injection, flow, and mixing of CO_2 in porous media with residual gas. Trans. Porous Med. 2011; 90:201-218. http://www.springerlink.com/content/e0pt67n28j264374/

12. Hosseini SA, Mathias SA, Javadpour F. Analytical model for CO_2 injection into brine aquifers-containing residual CH_4. Trans. Porous Med. 2012;94:795-815.

13. Cramer SD. The solubility of methane, carbon dioxide and oxygen in brines from 0 to 300 ˚C. U.S. Bureau of Mines Report. 1982; 8706.

14. Duan Z, Miller N, Weare J. An equation of state for the CH_4-CO_2-H_2O system: I. Pure systems from 0 to 1000°C and 0 to 8000 bar. Geochim Cosmochim Ac. 1992;56:2605-2617.

15. Kiepe J, Horstmann S, Fischer K, Gmehling J. Experimental determination and prediction of gas solubility data for methane + water solutions containing different monovalent electrolytes. Ind. Eng. Chem. Res. 2003;42:5392-5398.

16. Kiepe J, Horstmann S, Fischer K, Gmehling J. (Corrected Table 9) Ind. Eng. Chem. Res. 2004;43:3216 (Additions and Corrections to Ind. Eng. Chem. Res. 42:21).

17. Qin J, Rosenbauer RJ, Duan Z. Experimental measurements of vapor-liquid equilibria of the H_2O + CO_2 + CH_4 ternary system. J. Chem. Eng. Data. 2008;53:1246-1249.

18. Spycher N, Pruess K. A phase-partitioning model for CO_2–brine mixtures at elevated temperatures and pressures: Application to CO_2-enhanced geothermal systems. Trans. Porous Med. 2010;82(1):173-196.

19. Oldenburg CM, Lewicki JL. On leakage and seepage of CO_2 from geologic storage sites into surface water. Env. Geol. 2006;50(5):691-705.

20. Roache PJ. Computational fluid dynamics. Computational Fluid Dynamics, Albuquerque: Hermosa;1976:1.

21. Pruess K, Oldenburg CM, Moridis GJ. TOUGH2 User's Guide Version 2. Lawrence Berkeley National Laboratory Report LBNL-43134, 1999; and LBNL-43134 (revised), 2011.

22. Van Genuchten, M Th. A closed-form equation for predicting the hydraulic conductivity of unsaturated soils. Soil Sci Soc Am J. 1980;44.5: 892-898.

23. Corey AT. The interrelation between gas and oil relative permeabilities. Producers monthly. 1954;19.1: 38-41.

24. Spycher N, Pruess K. A phase-partitioning model for CO_2–brine mixtures at elevated temperatures and pressures: Application to CO_2-enhanced geothermal systems. Trans. Porous Med. 2010;82(1):173-196.

25. Taggart I. Extraction of dissolved methane in brines by CO_2 injection: Implication for CO_2 sequestration. Soc. Pet. Eng. 2009;SPE-12460.

26. Van Genuchten M Th. A closed-form equation for predicting the hydraulic conductivity of unsaturated soils. Soil Sci Soc Am J. 1980;44.5: 892-898.

DISCLAIMER

This document was prepared as an account of work sponsored by the United States Government. While this document is believed to contain correct information, neither the United States Government nor any agency thereof, nor The Regents of the University of California, nor any of their employees, makes any warranty, express or implied, or assumes any legal responsibility for the accuracy, completeness, or usefulness of any information, apparatus, product, or process disclosed, or represents that its use would not infringe privately owned rights. Reference herein to any specific commercial product, process, or service by its trade name, trademark, manufacturer, or otherwise, does not necessarily constitute or imply its endorsement, recommendation, or favoring by the United States Government or any agency thereof, or The Regents of the University of California. The views and opinions of authors expressed herein do not necessarily state or reflect those of the United States Government or any agency thereof or The Regents of the University of California.

Ernest Orlando Lawrence Berkeley National Laboratory is an equal opportunity employer.